IEEE Access
Multidisciplinary | Rapid Review | Open Access Journal

Received November 28, 2019, accepted December 26, 2019, date of publication December 30, 2019,
date of current version January 8, 2020.

Digital Object Identifier 10.1109/ACCESS.2019.2963117

Analysis of Current Distortion of Three-Phase Voltage Source Rectifiers and Its Application in Fault Diagnosis

CHUNSONG SUI, YIGANG HE, (Member, IEEE), AND MINGYUN CHEN
School of Electrical Engineering and Automation, Wuhan University, Wuhan 430072, China

Corresponding author: Yigang He (18655136887@163.com)

This work was supported in part by the National Natural Science Foundation of China under Grant 51977153, Grant 51977161, and Grant 51577046, in part by the State Key Program of National Natural Science Foundation of China under Grant 51637004, in part by the National Key Research and Development Plan "Important Scientific Instruments and Equipment Development" under Grant 2016YFF0102200, and in part by the Equipment Research Project in Advance under Grant 41402040301.

ABSTRACT The open-switch fault of three-phase voltage source rectifiers (VSR) may lead to ac current distortion. In the past decade, some current-based fault diagnosis methods have been proposed, which directly used the phenomenon of current distortion but lacked a detailed analysis of the cause of it. In this paper, the current distortion of VSR with unity power factor operation is analyzed from two aspects: the effect of the three-phase switching state on the ac current and the response of the VSR control system after the fault. Besides, the impact of the VSR system and control parameters on the current distortion is also discussed. The analysis verifies the feasibility of the distortion current for fault diagnosis, providing a theoretical basis for current-based fault diagnosis methods of VSRs. To substantiate the analysis of the distorted current, we designed a simplified fault diagnosis method, which determined the faulty phase by the difference of the normalized three-phase distorted current, and located the faulty switch by the grid voltage angle. The experiments are conducted to verify the analysis of current distortion and the reliability of the proposed fault diagnosis method.

INDEX TERMS Voltage source rectifier, open-switch fault, current distortion, fault diagnosis, SVPWM.

I. INTRODUCTION

Three-phase voltage source rectifiers (VSRs) are widely used in industrial applications because they can provide sinusoidal input current with unity power factor and constant dc bus voltage [1], [2]. Nevertheless, the capacitors, sensors, semiconductor devices (and their solder), control circuit and other components are prone to suffer electrical faults because of the complex operating environment of the rectifiers. According to the report, 34% of converter system failures are caused by power device faults, including semiconductor failures and soldering failures [3], [4].

Power device faults can be broadly categorized into short-circuit faults and open-switch faults [5]. The effect of short-circuit faults on the VSR is destructive. Nowadays, short-circuit fault detection has become a standard feature of the drive system, the over-current caused by short-circuit fault will trigger the protection devices and the drive system will shut down immediately. However, the open-circuit faults are often ignored by the protection devices since they are usually manifested as distorted ac current and do not show significant overcurrent. Compared with short-circuit faults, open-switch faults have a less significant influence on the system and can remain undetected for an extended period of time. But the switches that are still working will bear more voltage stress, which may lead to the secondary failure with more serious consequences and the system needs higher maintenance costs. In order to meet the requirements of the reliability in industrial applications, it is necessary to diagnose open-switch faults of the VSRs [6].

The conventional diagnosis methods applied in voltage source converter (including inverter and rectifier) and a brief comparison of different methods are shown in Table. 1.

The knowledge-based method proposed in [9] used a neural network to find the faulty switch. Knowledge-based diagnosis is also called data-driven fault diagnosis because

The associate editor coordinating the review of this manuscript and approving it for publication was Reinaldo Tonkoski.

TABLE 1. A comparison of different fault diagnosis methods.

Method [7], [8]	Advantages	Disadvantages
Knowledge-based [9], [10]	Reliable	Complicated during the process; Require large amounts of historical data
Model-based [11]–[13]	Fast	Sensitive to noises and system parameters; Require accurate mathematical model
Voltage-based [14]–[18]	Fast; Simple	Costly: require additional hardware to get the voltage signal
Current-based [19]–[29]	Simple; Economical	Sensitive to the current change

the intelligent techniques usually need a large volume of historical data [10]. This also means that Knowledge-based diagnosis methods are often complicated and require better controllers.

The model-based diagnosis method proposed in [11] used the current residual vector, which is the difference between the measured current and the estimated current and should be zero under normal condition, to achieve the fault diagnosis. Model-based diagnosis methods can complete the fault diagnosis quickly, but require an accurate mathematical model to get the estimated current [12], [13]. In addition, it is sensitive to noises and system parameters.

The voltage-based methods are usually simple but need additional sensors or hardware to obtain the voltage signals that are sensitive to the switching state [14], [15]. The method proposed in [16] used three extra voltage sensors to measure the ''pole voltages'', which are the voltages of each phase in respect to the dc middle point. By comparing the measured pole voltages and the estimated pole voltages obtained by the switching state, the faulty switch can be detected within 10 us. In order to avoid the high cost and complexity of voltage sensors, a simple hardware circuit was used to obtain the voltage signal indirectly [17], [18].

Compared with the aforementioned methods, the current-based methods are relatively simple and directly use the existing ac current signals without the need for additional sensors (or hardware). Therefore, current-based methods have been widely studied [19]–[22].

The current Park's vector approach was employed for diagnosing voltage source inverter faults in [23], which is the basis of many diagnosis methods [24]. The major drawback of the methods in [23], [24] is the load dependence. The setting of parameters (such as some thresholds) in the diagnosis algorithm is related to the load current. In order to make the fault detection independent of the load, [25] suggested using the normalized current instead. To achieve this, the first order harmonic coefficients of ac current are used as the reference values, which are computed by means of a DFT. Another way to get rid of the drawback of load dependence is to use load-independent parameters for fault diagnosis, such as the angle of the current Park's vector. The method proposed in [26] combined a detection method based on the derivative of the current Park's vector angle with a localization method based on the current polarity, which could be used both in voltage source inverters and VSRs.

In recent years, more and more attention has been paid to the fault diagnosis of VSRs. Based on symmetry analysis in healthy and faulty conditions, a fault detection and location method was proposed in [27]. This method could detect multiple open-switch faults. But it required more calculation. The proposed method in [28], [29] employed current distortion to diagnose open-switch faults. By detecting the zero-crossing characteristics to identify the faulty phase, and detecting the current of the non-faulty phase to locate the faulty switch, this method could reduce the required diagnostic calculations.

The current-based fault diagnosis methods of VSRs are mostly based on the analysis of the distorted current after the fault. But most of the methods directly used this distorted phenomenon and neglected a detailed analysis of the causes of the current distortion. When the open-switch fault occurs, both positive and negative current can flow since the VSRs mainly complete the energy transformation through the diodes. But there will be two serious distorted sections, in which the current of the faulty phase remains nearly zero. This phenomenon is the focus of this study, which occurs as well when using three-phase diode rectifiers. In this paper, the two sections with the most serious current distortion are called zero sections, which are divided into the first zero section (ZS1) and the second zero section (ZS2) according to their relationship with the faulty switches.

The existence of zero sections is the indispensable basis of all current-based diagnosis methods, but there is no article to give a detailed analysis of that. To fill in the research gap, this study is proposed. This paper, taking the VSR with the double closed-loop control system and SVPWM modulation method as an example, analyzes the current distortion after the open-switch fault from two aspects: the effect of the three-phase switching state on the three-phase current and the response of the VSR control system after the fault [30]. Although these two sections have been widely used in current-based fault diagnosis for VSR. It is the first time to analyze the causes of the zero sections and the duration of ZS1 and ZS2. In addition, we designed a simplified fault diagnosis method and verified by experiments to bolster the analysis of the current distortion.

II. ANALYSIS OF AC CURRENT IN NORMAL AND ABNORMAL CONDITIONS

The structure and control strategy of the three-phase VSR are shown in Fig. 1. Here, e_a, e_b, e_c are the grid voltage, v_a, v_b, v_c are the ac side voltage of VSR, i_a, i_b, i_c are the ac current, L is the ac filter inductance, C is the dc-link capacitance, R_L is the load and U_{dc} is the dc-link voltage. There are 6 IGBTs (S_1-S_6), including the anti-parallel diode (D_1-D_6) in corresponding.

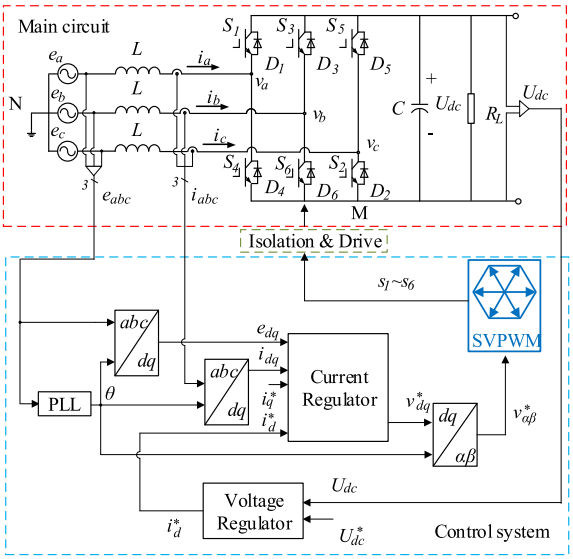

FIGURE 1. VSR system.

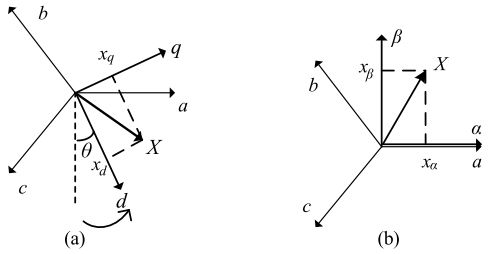

FIGURE 2. The transformation of reference frames. (a) The relationship of *abc* and *d-q* reference frame. (b) The relationship of *abc* and *α-β* reference frame.

The double closed-loop control system and the SVPWM modulation strategy are mostly adopted in engineering. The voltage regulator controls the dc voltage (U_{dc}) and stabilizes it at the reference dc voltage (U^*_{dc}). In order to operate with unity power factor, the reference of q-axis current (i^*_q) is set as 0, while the reference of d-axis current (i^*_d) is set as the output of the voltage regulator. The voltage control signals v^*_d and v^*_q are obtained through the current regulator, and then converted into v^*_α and v^*_β for SVPWM generator.

There are three reference frames involved in this paper, namely the three-phase *abc* reference frame, the synchronously rotating d-q reference frame and the two-phase stationary α-β reference frame. The relationships between the three reference frames are shown in Fig. 2. Here, θ is the grid voltage angle (calculated by PLL) and X is the rotation vector, specifically, grid voltage vector E, control vector V^* and ac current vector I. It is important to note that the d-axis is 90° behind a-axis at the initial time in this paper.

The working states of switches (including IGBTs and diodes) are determined by the direction of ac current and control signals. Consider the direction of i_a, the working states of the switches with V2(110) and V0(000) are shown in Fig. 3. For phase a, the positive current flows through the S_4 and D_1, and the negative current flows through the S_1 and D_4.

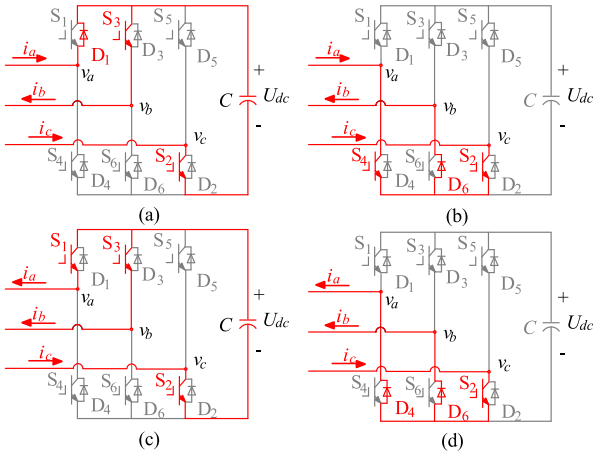

FIGURE 3. The working states of the switches. (a) $i_a > 0$, $V_2(110)$. (b) $i_a > 0$, $V_0(000)$. (c) $i_a < 0$, $V_2(110)$. (d) $i_a < 0$, $V_0(000)$.

The VSRs can operate with sinusoidal ac current, but the current will be distorted when an open-switch fault occurs. When the VSR is operating with unity power factor, the comparison of ac current before and after the S_1 open-switch fault is shown in Fig. 4(a). The positive half-cycle of i_a is not affected by the fault because the positive current flows through S_4 or D_1 rather than S_1. By contrast, the S_1 open-switch fault causes current distortion in the negative half-cycle, because the negative current cannot flow through the upper arm. As a result, there are two sections in which the current is nearly zero in the beginning and the end of the negative half-cycle. Contrasting to the S_1 open-switch fault, S_4 open-switch fault does not affect the negative half-cycle of i_a, but causes two distortion sections in the positive half-cycle.

In the distorted sections, i_a is nearly zero, so they are called zero sections in this paper. In order to distinguish the two distorted sections, the section in the beginning of the half-cycle where the faulty switch should work is called the first zero section (ZS1), and the other is called the second zero section (ZS2). To further explain, S_1 only works in the negative half-cycle of i_a, so the distorted section in the beginning of the negative half-cycle of i_a is ZS1.

Current-based fault diagnosis methods for VSR are mostly based on the analysis of ac current in zero sections, which are the sections of the most serious current distortion and provide vital information of the fault. Some studies analyze the behavior of the freewheeling diode in the faulty phase from the perspective of the grid voltages. Take phase a as an example, it is considered that only when e_a is lower than e_b and e_c can the negative half-cycle of i_a flow through D_4. Therefore, the two zero sections, both of which last 30°, have the same duration (t_{ZS1} and t_{ZS2}) [20]. But in reality, t_{ZS1} and t_{ZS2} are different after the open-switch fault as shown in Fig. 4, and t_{ZS1} is longer than t_{ZS2}.

The time threshold T_{th} plays a key role in current-based fault diagnosis methods. When the duration of the abnormal state exceeds the T_{th}, the fault is identified. Therefore the T_{th} needs to be set reasonably. On the one hand, if T_{th} is too short,

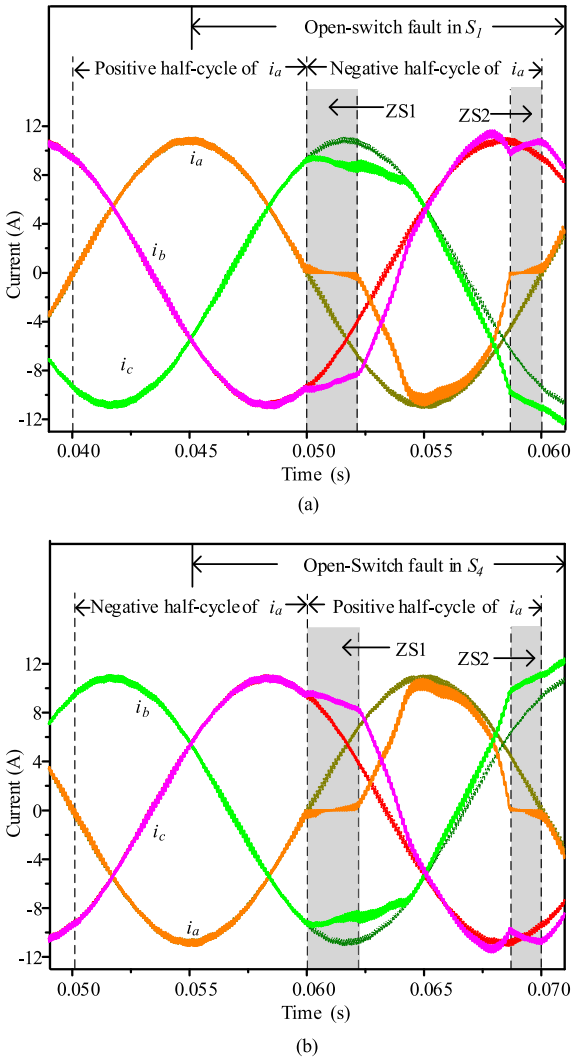

FIGURE 4. Current before and after an open-switch fault. (a) S_1 open-switch fault. (b) S_4 open-switch fault.

it may cause misdiagnosis due to switching noise and sensing error. On the other hand, if T_{th} is too long, it may lead to the failure of the diagnosis.

In current-based fault diagnosis methods, the design of T_{th} depends on the zero sections, the t_{ZS1} and t_{ZS2} will affect the efficiency and reliability of the fault diagnosis. Therefore, it is necessary to analyze the two zero sections.

III. ANALYSIS OF ZERO SECTIONS

In order to analyze the reason of ac current distortion after the open-switch fault, it is necessary to know how the current changes under normal conditions. In this paper, the grid frequency (f_0) is 50 Hz, and the sampling/switching frequency (f_s) is 10 kHz.

Two switching periods ($T_s = 1/f_s = 0.1$ ms) are selected for analysis: 1) when i_a is max, $\theta = 90°$; 2) when i_a enters negative half-cycle, $\theta = 180°$. The change of i_a, the control signals (s_a, s_b, s_c), the basic space vectors (V_ns) and the relationship between E and V^* are shown in Fig. 5.

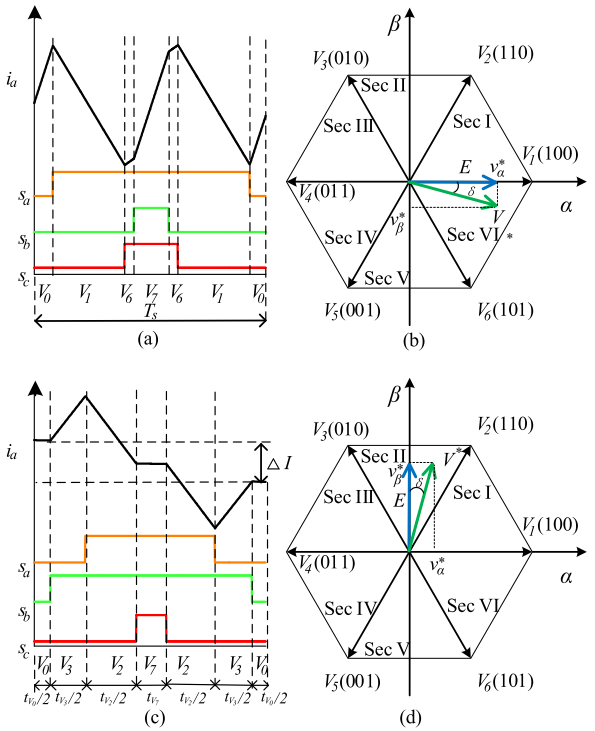

FIGURE 5. Current analysis under normal working conditions. (a) The relationship of i_a and V_n when $\theta = 90°$. (b) E and V^* when $\theta = 90°$. (c) The relationship of i_a and V_n when $\theta = 180°$. (d) E and V^* when $\theta = 180°$.

In the 7-segment SVPWM strategy, as is indicated in Fig. 5(a) and Fig. 5(c), the change of i_a is determined not only by s_a, but also by s_b and s_c. Therefore, in a switching period, i_a can be regarded as a piecewise linear function consisting of seven segments, the change of i_a can be calculated by the slope ($k^a_{V_n}(\theta)$) and the time (t_{V_n} or $t_{V_n}/2$) of each segment. In this paper, the $k^a_{V_n}(\theta)$ is defined as the effect of V_n on the three-phase current, and the t_{V_n} is the action time of V_n in a switching period. Take Fig. 5(c) ($\theta = 180°$) as an example, since the switching state in the 7-segment SVPWM strategy is symmetrical, the change of i_a in a switching period can be calculated by using (1):

$$\Delta I = k^a_{V_0} t_{V_0} + k^a_{V_2} t_{V_2} + k^a_{V_3} t_{V_3} + k^a_{V_7} t_{V_7} \tag{1}$$

Therefore, the causes of zero sections should be analyzed from two aspects: the effect of V_n on the three-phase current ($k^a_{V_n}$) and the response of the control system after the fault, which determines the t_{V_n}.

Fig. 5(b) and Fig. 5(d) show that V^* always lags behind E by an angle δ. From the perspective of power transmission ($P = EV \sin(\delta)/\omega L$), δ is inevitable, and its value is related to the load power and L.

A. THE EFFECT OF BASIC SPACE VECTORS ON CURRENT

The voltage equation of VSR based on Kirchhoff's voltage law is described as (2):

$$L\frac{\mathrm{d}i_x}{\mathrm{d}t} + Ri_x = e_x - U_{dc}s_x - U_{\mathrm{MN}} \tag{2}$$

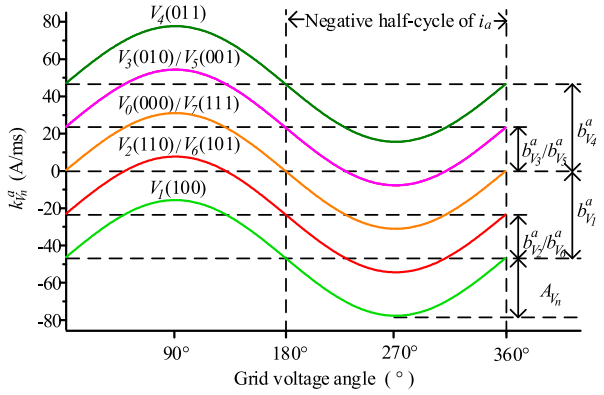

FIGURE 6. The effect of V_n on i_a.

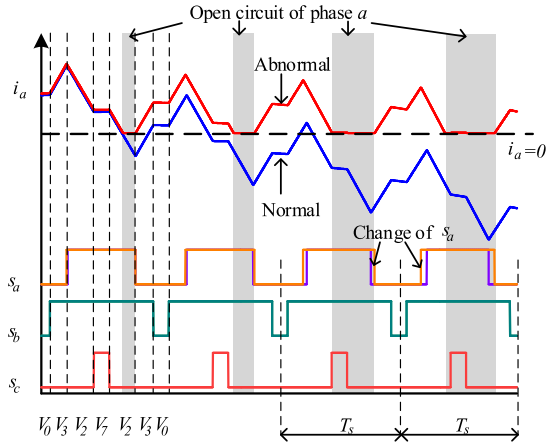

FIGURE 7. The comparison between the faulty and normal conditions of i_a and control signals.

where, x (= a, b, c) is the index for three-phase; R is the corresponding resistance of L; N denotes the ground, M denotes the negative pole of U_{dc}, according to the symmetry of VSR, the voltage U_{MN} can be obtained by (3):

$$U_{\mathrm{MN}} = -\frac{s_a + s_b + s_c}{3} U_{dc} \tag{3}$$

To simplify the analysis, in a switching period, the U_{dc} is considered to be stable and the effect of R is neglected. Therefore, the effect of V_n on ac current can be expressed as (4):

$$k^x_{V_n}(\theta) = \frac{\mathrm{d}i_x}{\mathrm{d}t} = A\sin(\theta + \varphi_x) + b^x_{V_n} \tag{4}$$

where, n (= 0, 1, 2, 3, 4, 5, 6, 7) is the index of the eight basic space vectors; A is the ratio of grid voltage amplitude to L; φ_x is the initial phase of three-phase voltage; $b^x_{V_n}$ is related to U_{dc}, L and V_n. Take $V_1(100)$ as an example, U_{MN} = - U_{dc} / 3, $b^a_{V_1} = -2U_{dc}$ / (3L).

The $k^a_{V_n}$ is shown in Fig. 6, when the grid voltage is 220 V, U_{dc} is 700 V, and L is 10 mH.

Combined with the analysis in Section II and Fig. 6, it can be concluded that after S_1 open-switch fault, $V_1(100)$, $V_2(110)$, $V_6(101)$ and $V_7(111)$ cannot work in the negative half-cycle of i_a, which are thought to result in the decrease of i_a. Simultaneously, only $V_0(000)$, $V_3(010)$ and $V_5(001)$ can decrease i_a. By comparing $k^a_{V_0}$, $k^a_{V_3}$ and $k^a_{V_5}$, it can be found that when i_a is negative, the decrease of i_a is mainly caused by V_0 after S_1 open-switch fault.

It is worth noting that in the range of two aforementioned zero sections, $|k^a_{V_0}(\theta)|$ is small, and the ability of V_0 to decrease i_a is weak. While in the midpoint of the negative half-cycle of i_a ($\theta = 270°$), $|k^a_{V_0}(\theta)|$ is large, and the ability of V_0 to decrease i_a is strong.

The analysis of V_0 also proves that when S_1 open-switch fault occurs, even if the e_a is not the lowest, the diode D_4 can still be switched on.

B. THE FORMATION OF ZERO SECTIONS

Take S_1 as an instance, Fig. 4(a) shows that ZS1 begins at $\theta = 180°$, ZS2 ends at $\theta = 360°$. Choosing four switching periods including a period before $\theta = 180°$ and three periods after $\theta = 180°$, the comparisons between abnormal condition and normal condition of i_a, control signals (s_a, s_b, s_c), and V_ns are shown in Fig. 7.

As shown in Fig. 5(d), the control vector V^* is in Sec II, so V_3, V_2, V_0 and V_7 will work. In the switching period just before $\theta = 180°$, V_0 and V_7 make i_a increase, but the ability of that is relatively limited because $|k^a_{V_0}|$ is small, which is shown in Fig. 6. Correspondingly, in the several switching periods after $\theta = 180°$, V_0 will decrease i_a, but this effect is also limited. V_3 and V_2 make i_a increase and decrease, respectively. As shown in Fig. 6, $|k^a_{V_2}|$ and $|k^a_{V_3}|$ are almost the same when $\theta = 180°$. But with the increase of θ, the ability of V_3 to increase i_a will be weakened, while the ability of V_2 to decrease i_a will be enhanced.

As shown in Fig. 7, in the 7-segment SVPWM strategy, when S_1 is under the normal condition, the change of i_a in a switching period is: almost stable (V_0) → increase (V_3) → decrease (V_2) → almost stable (V_7) → decrease (V_2) → increase (V_3) → almost stable (V_0). The i_a decreases in a switching period because the operating time of V_2 (t_{V_2}) is longer than the operating time of V_3 (t_{V_3}).

When S_1 open-switch fault occurs and i_a is still positive, the fault of S_1 has no effect on i_a because S_1 does not work. However, as shown in Fig. 7, when i_a decreases to zero, it will remain at zero in the shaded bands instead of further decreasing, which means that the phase a is under open-circuit state. This is because after S_1 open-switch fault, the negative current of phase a can only flow through D_4. If D_4 is turned on, the $V_2(110)$ will become $V_3(010)$, whose effect is to increase i_a. But if the i_a increased from zero to some positive value, the V_2 would work normally and let the current decrease back to zero, therefore i_a will remain at zero anyway.

When the normal V_3 works, the current will increase. In a switching period, the i_a decreases slower than the normal condition because part of the V_2, whose effect is to decrease i_a, cannot work normally. With the increase of the θ, as shown in Fig. 7, the time for V_2 and V_7 to operate under open-circuit state increases, and the current is almost maintained at zero.

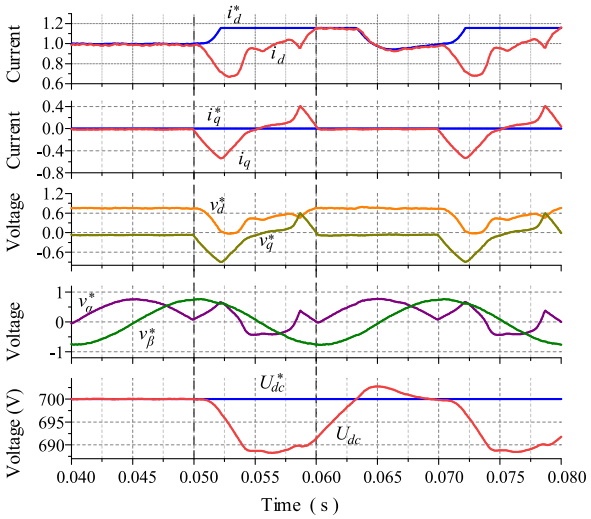

FIGURE 8. The parameters of the control system.

From what has been discussed above, it can be concluded that for S_1, the beginning of ZS1 is caused by the changes of i_a from positive to negative. The reason for the persistence of ZS1 is that some basic space vectors, which decrease the current, cannot work normally (such V_2 and V_7), and at this time only V_0 can make i_a normally decrease, but the small value of $|k^a_{V_0}|$ means that its ability to decrease i_a is weak.

The reason for the end of ZS2 is contrary to that for the beginning of ZS1, that is, the i_a changes from negative to positive. The analysis is similar to the above discussions.

In Fig. 7, it is worth noting that the s_a in the abnormal condition is slightly different from that in the normal condition, namely after an open-switch fault occurs, the VSR control system will respond and change the control vector V^*. So it is necessary to analyze the performance of the control system after the fault. When the S_1 open-switch fault occurs at 0.045s, the changes of the main parameters of the control system (in addition to the dc voltage, other parameters are per-unit values) are shown in Fig. 8.

After S_1 open-switch fault, and when $\theta = 180°$ (at 0.05s in Fig. 8), i_d and i_q will decrease because i_a remains at zero. Accordingly, the current regulator will respond, so v^*_d and v^*_q will decrease. For V^*, the v^*_α will gradually increase, as shown in Fig. 8. If S_1 is normal, this regulation will be effective, because the effect of V_2 is to decrease i_a and the increase of v^*_α means the increase of t_{V_2}. However, due to S_1 open-switch fault, $V_2(110)$ cannot work normally, so the regulation will not work. The i_a will continue to maintain near 0, thus i_d and i_q continue to decrease and v^*_α continues to increase. The continuous decrease of i_d and i_q will lead to a decrease of power supply from the grid to the load, leading to a decrease of U_{dc}. The voltage regulator will respond to increase the i^*_d. Under the joint action of the current and voltage regulators, the amplitude and angle of V^* will change. The comparison between normal and abnormal V^*s is shown in Fig. 9.

As can be seen from Fig. 9, due to the accumulation of the faults, V^* will cross from Sec II to Sec I inversely, when V_1, V_2, V_0 and V_7 play their roles.

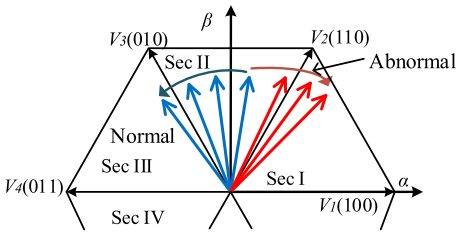

FIGURE 9. V^* in ZS1 of normal and abnormal conditions.

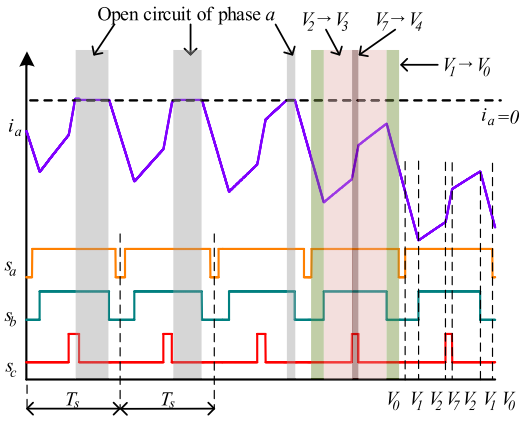

FIGURE 10. The end of ZS1.

Since S_1 cannot work normally, $V_7(111)$, which normally decreases the current, will change into $V_4(011)$, which increases i_a rapidly. $V_2(110)$ will change into $V_3(010)$, and in ZS1, V_3 usually increases i_a.

But at this time, $V_1(100)$ will change into $V_0(000)$, which can decrease i_a. The current and control signals when i_a leaves ZS1 are shown in Fig. 10.

As shown in Fig. 6, with the increase of θ, the ability of V_0 to decrease i_a is gradually enhanced, while the ability of V_4(changed from V_7) and V_3(changed from V_2) to increase the current is correspondingly weakened, so the time of V_7 and V_2 under the open-circuit state (the grey shaded bands in Fig. 10) will decrease.

When the V^* is in Sec I, considering the open-circuit state, the change of i_a in a switching period can be approximately expressed by (5):

$$\Delta I = \min(k^a_{V_0}(t_{V_0} + t_{V_1}) + k^a_{V_3} t_{V_2} + k^a_{V_4} t_{V_7}, 0) \qquad (5)$$

When $\Delta I < 0$, i_a leaves ZS1.

According to the above analysis, the end of ZS1 is jointly determined by the circuit state (determine $k^a_{V_n}$) and the control system (determine t_{V_n}), and $|k^a_{V_0}|(t_{V_0}+t_{V_1})$ plays a key role in the decrease of i_a. Furthermore, $|k^a_{V_0}|$ is related to θ, and the response of the control system is not instant, so $|k^a_{V_0}|(t_{V_0}+t_{V_1})$ cannot rapidly increase after ZS1 begins.

Increasing the gain of the current regulator can speed up the response of the control system and shorten the ZS1. However, the excessive gain will lead to the instability of the system, and it is not recommended to increase the gain too much. In conclusion, for a reasonably designed VSR that runs with

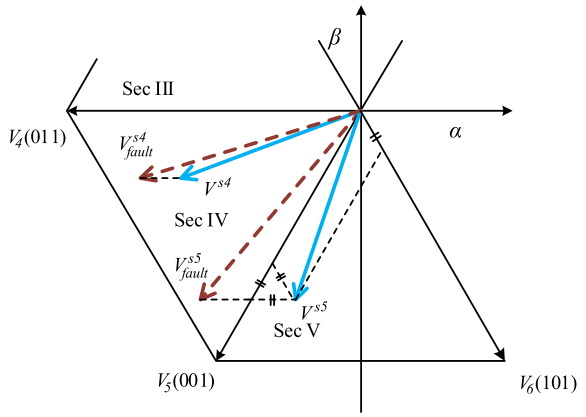

FIGURE 11. The influence of S1 open-switch fault on control vector V^*.

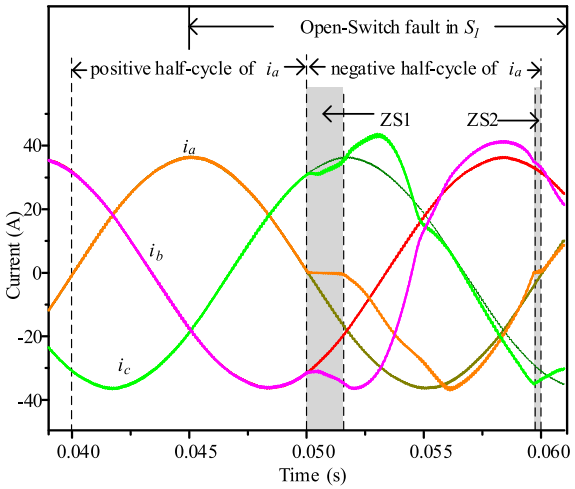

FIGURE 12. The current distortion with a large load.

unity power factor, ZS1 is inevitable after the open-switch fault, and it is feasible to use ZS1 for fault diagnosis.

At the end of this section, the reason why ZS2 begins will be discussed. In Sec IV, S_1 open-switch fault only affects $V_7(111)$, but in Sec V, $V_6(101)$ will also be affected. Therefore, the influences of S_1 open-switch fault on the V^* in Sec IV and Sec V need to be analyzed respectively, as shown in Fig. 11.

In Sec IV, it can be seen from Fig. 6 that the effect of V_4 is to increase i_a; the effect of V_0 (and V_7) is to decrease it. Whereas the effect of V_5 is relatively complex, it can make i_a increase or decrease. But $|k_{V_5}^a|$ is small, so V_5 has a less significant effect on the current.

When S_1 open-switch fault occurs, $V_7(111)$ fails to work properly and changes into $V_4(011)$. The amplitude of the V^* increases and the angle decreases, as shown in Fig. 11, V^{s4} will work as V_{fault}^{s4}. As V_7 changes into $V_4(011)$, i_a will increase, so the control system will respond to decrease the current. Specifically, it will decrease the amplitude of V^* (by increasing t_{V_0} and t_{V_7} to decrease the current) and accelerate the increase of the angle (increases t_{V_5} and decreases t_{V_4}).

At this time, $|k_{V_0}^a|$ is large, that is, the ability of V_0 to decrease the current is strong. Therefore, even if V_7 cannot work normally, V_0 can inhibit the rapid increase of i_a, and the adjustment of the control system can still play a role.

But in Sec V, V_7 will change into V_4, and $V_6(101)$ will fail to work and change into $V_5(001)$, which has a huge impact on V^*. As shown in Fig. 11, V^{s5} will work as V_{fault}^{s5}, due to S_1 open-switch fault. At this point, i_a will increase rapidly, and the regulation of the control system will decrease the amplitude of V^* and accelerate the increase of the angle. But $|k_{V_0}^a|$ is small, and $|k_{V_5}^a|$, $|k_{V_4}^a|$ are relatively large, that is, V_0 will not be able to inhibit the increase of the current caused by V_5 and V_4 (changed from V_7), so the regulation of the control system will not work. The i_a continues to increase rapidly until it reaches 0, then enters ZS2.

The analysis shows that the beginning of ZS2 is still jointly determined by the circuit state (determine $k_{V_n}^a$) and control system (determine t_{V_n}). Since the regulation of the control system in Sec V is completely invalid, which will lead to i_a rapidly increase, the entering of the V^* into Sec V can be seen as the reason for the beginning of ZS2.

ZS2 begins when the V^* enters into Sec V, and ends when $\theta = 360°$. Therefore, when the lag angle δ increases, the duration of ZS2 will decrease. Fig. 12 shows the current after the dc load is increased while other parameters remain unchanged. Compared with Fig. 4(a), it is obvious that the ZS2 is shorter when the ac current is larger.

Finally, for VSR with unity power factor operation, the two zero sections of S_1 open-switch fault are summarized and compared as shown in Table. 2.

The two zero sections are distributed at both ends of the negative half-cycle of i_a. According to the analysis in this section, the main reason why i_a cannot decrease normally in the zero sections after S_1 open-switch fault is that the effect of V_0, which is the only reason why i_a decreases, is offset by the effect of other fault space vectors which make i_a increase since $|k_{V_0}^a|$ is small.

By comparing the duration of the two zero sections, it can be found that ZS1 is generally longer, while ZS2 is shorter. Through the analysis of time threshold T_{th}, it can be concluded that the design of the T_{th} in the current-based diagnosis method for VSR with unity power factor operation should aim to realize the diagnosis of ZS1. Since, in the operating state, the change range of ZS1 is limited, while the change range of ZS2 is flexible. Additionally, for operating equipment, the parameters of the equipment and the control system are generally fixed, but the current is changeable.

In sum, the analysis in this section focuses on the S_1 open-switch fault. For other switch faults, they are similar to that of S_1 and therefore do not need to be elaborated.

IV. A SIMPLIFIED FAULT DIAGNOSIS METHOD BASED ON ZERO SECTIONS

In this section, a simplified fault diagnosis method for VSR with unity power factor operation is proposed to verify the above analysis of zero sections, and the effectiveness of the proposed method is verified through experiments.

TABLE 2. The comparison between ZS1 and ZS2 of S_1 open-switch fault.

Zero section	Beginning reason	End reason	Duration	Main relevant factors
ZS1	i_a: positive→negative	$\lvert k^a_{V_0}\rvert(t_{V_0}+t_{V_1})>k^a_{V_3}t_{V_2}+k^a_{V_4}t_{V_7}$	Long	Response speed of control system
ZS2	V^* enters Sec V	i_a: negative→positive	Short	Lag angle δ of V^*

TABLE 3. Location of the faulty switch.

Faulty switch	Phase	Half cycle	Angle
S_1	A	Negative	180°-360°
S_4	A	Positive	0°-180°
S_3	B	Negative	300°-360°,0°-120°
S_6	B	Positive	120°-300°
S_5	C	Negative	60°-240°
S_2	C	Positive	240°-360°,0°-60°

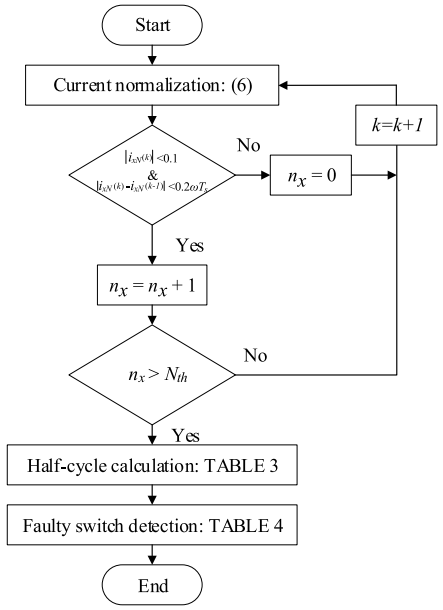

FIGURE 13. Flowchart of the proposed diagnosis method.

A. FAULT DIAGNOSIS METHOD

The location of zero sections could be used to locate the faulty switch, as shown in Table. 3, S_1 open-switch fault causes zero sections in the negative half-cycle of i_a, while S_4 causes zero sections in the positive half-cycle of i_a. Accordingly, S_3 and S_6 cause zero sections in i_b, while S_5 and S_2 cause zero sections in i_c.

Based on the position of zero sections, a simplified fault diagnosis method is proposed in this paper. The advantages of the proposed method are that it is independent of the load, the requirement for calculation is not so demanding, the signals used are all from the control system, which means that no extra sensors are required. The flowchart of the proposed fault diagnosis method is shown in Fig. 13, which mainly includes ac current normalization, zero-value detection, faulty phase detection and half-cycle detection.

There are five steps for fault diagnosis.

Step 1. Normalize three-phase current. When the load changes, the load current will change accordingly. Normalizing the current can reduce the dependence of fault diagnosis on the load. The i_d and i_q in the control system can be used as the reference value, and the normalized current can be calculated by (6):

$$i_{xN} = \frac{i_x}{\sqrt{i_d^2 + i_q^2}} \tag{6}$$

where $x(= a, b, c)$ is the index for three-phase; i_{xN}s are the normalized current, which are sinusoidal waves with the amplitude of 1.

Step 2. Detect whether i_{xN} has a zero-value, and give the signal z_x when the zero-value is detected. To improve the accuracy of detection, the zero-value is jointly determined by the amplitude and derivative of i_{xN}. In the normal condition, when the current goes zero (the direction of current changes), the absolute derivative of i_{xN} is ω (when $f_0 = 50$ Hz, $\omega = 100\pi$). In the zero sections, the absolute derivative of i_{xN} is almost zero, so the threshold of the amplitude can be set as 0.1, and the threshold of the derivative can be set as 0.2ω, that is:

$$z_x = \begin{cases} 1, & |i_{xN}|<0.1 \text{ and } |\dfrac{di_{xN}}{dt}|<0.2\omega \\ 0, & \text{else} \end{cases} \tag{7}$$

Step 3. Give the fault phase signals F_x after the duration of z_x exceeds the time threshold T_{th}. From the analysis of Section III, the design of the T_{th} in diagnosis method of VSR should aim to realize the diagnosis of ZS1. The simulation results show that when the current frequency is 50 Hz, and the sampling/switching frequency is 10 kHz, the duration of ZS1 is generally longer than 1.5 ms, thus $T_{th} = 1$ ms is chosen. To achieve this step, three-phase counters are needed. When $z_x = 1$, the corresponding counter n_x counts, whereas when $z_x = 0$, the counter is cleared. Since the sampling frequency is 10 kHz, the comparison number $N_{th} = 10$ is chosen, when $T_{th} = 1$ ms. The detection can be expressed as (8):

$$F_x = \begin{cases} 1, & n_x > N_{th} \\ 0, & \text{else} \end{cases} \tag{8}$$

Step 4. Judge the positive or negative half-cycle h_x by grid voltage angle θ. The relationship between h_x and θ is shown in Table. 3, which can be expressed by (9):

$$h_x = \begin{cases} 1, & \text{positive half cycle of phase } x \\ 0, & \text{negative half cycle of phase } x \end{cases} \tag{9}$$

TABLE 4. Signals of the faulty switch.

Faulty switch	F	F_x	h_x
S_1	1	F_a=1	h_a=0
S_4	4	F_a=1	h_a=1
S_3	3	F_b=1	h_b=0
S_6	6	F_b=1	h_b=1
S_5	5	F_c=1	h_c=0
S_2	2	F_c=1	h_c=1

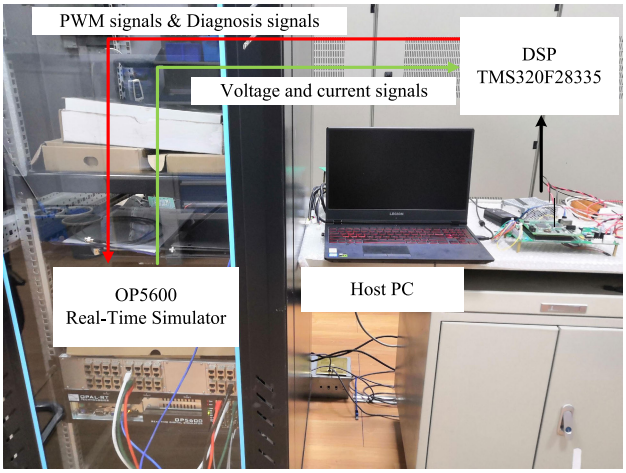

FIGURE 14. The experimental setup based on RT-LAB.

TABLE 5. Parameters of the VSR system.

Parameters	Symbols	Value
Grid voltage	e_a, e_b, e_c	220 V
Grid frequency	f_0	50 Hz
DC-kink voltage	U_{dc}	700 V
Sampling/Switching frequency	f_s	10 kHz
Filter inductance	L	10 mH
DC-kink capacitance	C	470 μF
Load power	P	5 kW/20 kW

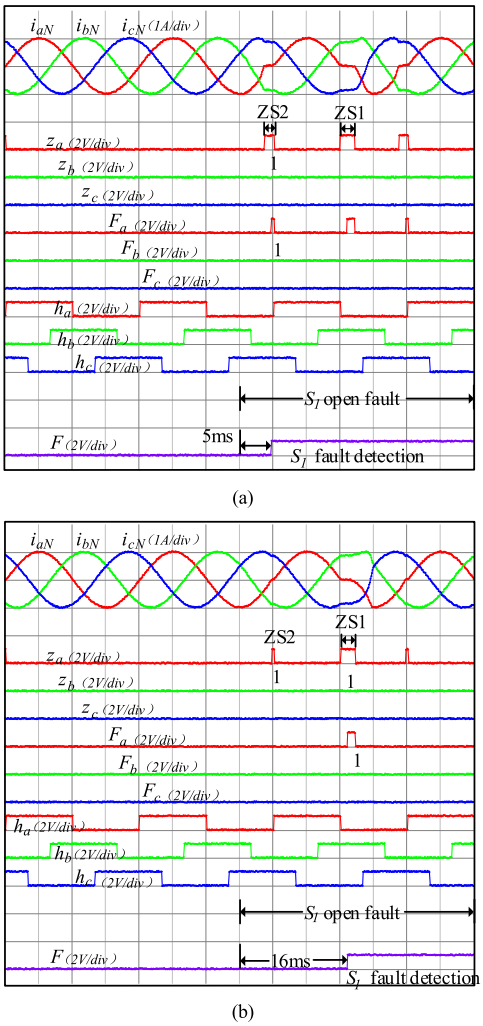

FIGURE 15. Experimental results of fault diagnosis after S_1 open-switch fault occurs when the grid voltage is 220V and the dc-link voltage is 700V. (a) DC load of 5kW. (b) DC load of 20kW.

Step 5. Locate the fault switch and output the fault location signal F by F_x and h_x. Take S_4 open-switch fault as an example, $F_a = 1$ means the switches of phase a may have a fault. If $h_a = 1$ is detected at this time, S_4 open-stitch fault can be determined. The rules of each switch are shown in Table. 4.

The fault diagnosis method proposed in this paper only requires three-phase current signals i_{abc}, the d-q axis current signal i_{dq}, and the grid voltage angle θ, which are all from the control system and do not need additional sensors. This diagnosis method can basically complete the fault diagnosis within half a cycle (10ms). But when ZS2 is relatively short, it needs one cycle to complete the fault diagnosis.

B. EXPERIMENTAL RESULTS

In this section, the analysis of two zero sections in Section III is verified by experiments. At the same time, the reliability of the simplified fault diagnosis method proposed in this section is verified.

The experimental setup is shown in Fig. 14, consisting of a real-time laboratory (RT-LAB) test platform OP5600, a control board TMS320F28335, and a host computer. The main circuit includes the grid voltage sources, the converter and the load are realized by the RT-LAB simulator. The control board receives voltage and current signals through A/D conversion interface, outputs PWM control signals to the RT-LAB simulator. The fault diagnosis method is realized by the control board, the diagnosis signals are sent to the RT-LAB simulator and showed by the host computer. Thanks to the advantages of the RT-LAB platform, it is convenient to change the values of the main circuit parameters, thus to verify the difference between the two zero sections under disparate operation conditions and the reliability of the proposed method. Fig. 15 shows the current and diagnosis signals after the fault. The difference between Fig. 15(a) and (b) is the load power, which is 5kW and 20kW, respectively. The details of the experimental setting are shown in Table. 5.

Fig. 15 shows the normalized ac current i_{aN}, i_{bN}, i_{cN}, three-phase zero-value signals z_a, z_b, z_c, three-phase fault signals F_a, F_b, F_c, three-phase positive and negative half-cycle

signals h_a, h_b, h_c, and faulty switch signal F. In the normal condition, the normalized three-phase current are almost sinusoidal signals, the three-phase zero-value signal and the three-phase fault signal are 0. When S_1 open-switch fault occurs in the negative half-cycle of i_a, at the end of this half-cycle (ZS2), the current distortion is the most obvious. When i_a is maintained at 0, the zero-value signal of phase a is 1 ($z_a = 1$), while z_b and z_c are still maintained at zero. When the duration of $z_a = 1$ exceeds the T_{th}, fault signal of phase a is 1 ($F_a = 1$) and that means an open-switch fault of phase a occurs. At this time, the positive and negative half-cycle signal is 0 ($h_a = 0$), as can be seen from Table. 4, S_1 open-switch fault occurs.

From the change of z_a in Fig. 15, it can be seen that the length of the two zero sections is different. When the load is large, the length of ZS2 will be shortened, which is consistent with the conclusion of Section III. It can be seen from Fig. 15 that when ZS2 lasts for a long time, the diagnosis can be completed within half a cycle. However, when the duration of ZS2 is shorter than T_{th}, the diagnosis needs to be postponed and will complete through the ZS1 of the next negative half-cycle of i_a. The diagnosis will take longer than half a cycle, but can be completed within a cycle.

By contrast, the shorter ZS2 can be used for diagnosis by reducing the T_{th}, but when T_{th} is small, switch noise and sensor error may lead to misdiagnosis, which is unacceptable. However, fortunately, the shorter ZS2 also means that the current distortion and voltage distortion in ZS2 are not serious, so the increase of diagnostic time has a less impact on the power grid and load. Therefore, it is acceptable for us not to conduct diagnosis for this scenario.

V. CONCLUSION

This paper analyzes the open-switch fault of VSR with unity power factor operation from the effect of the V_ns on the three-phase current and the response of the control system after the fault. Besides, the causes, duration and main relevant factors of the two most serious current distortion sections, which are called ZS1 and ZS2, respectively, are also discussed.

The feasibility of zero sections for fault diagnosis is analyzed, which provides a theoretical basis for the current-based diagnosis method. In this work, it is concluded that the design of the T_{th} in diagnosis method for VSR with unity power factor operation should aim to realize the diagnosis of ZS1. Thus, a simplified fault diagnosis method is proposed. The advantages of this method are that it is independent of the load current, the signals used are all control signals, and the calculation requirement is not so demanding.

REFERENCES

[1] V. Blasko and V. Kaura, "A new mathematical model and control of a three-phase AC–DC voltage source converter," *IEEE Trans. Power Electron.*, vol. 12, no. 1, pp. 116–123, Jan. 1997.

[2] J.-C. Kim, J.-C. Park, and S. Kwak, "Predictive direct power control technique for voltage source converter with high efficiency," *IEEE Access*, vol. 6, pp. 23540–23550, 2018.

[3] S. Yang, D. Xiang, A. Bryant, P. Mawby, L. Ran, and P. Tavner, "Condition monitoring for device reliability in power electronic converters: A review," *IEEE Trans. Power Electron.*, vol. 25, no. 11, pp. 2734–2752, Nov. 2010.

[4] S. Yang, A. Bryant, P. Mawby, D. Xiang, L. Ran, and P. Tavner, "An industry-based survey of reliability in power electronic converters," *IEEE Trans. Ind. Appl.*, vol. 47, no. 3, pp. 1441–1451, May/Jun. 2011.

[5] B. Lu and S. Sharma, "A literature review of IGBT fault diagnostic and protection methods for power inverters," *IEEE Trans. Ind. Appl.*, vol. 45, no. 5, pp. 1770–1777, Sep./Oct. 2009.

[6] S.-M. Jung, J.-S. Park, H.-W. Kim, K.-Y. Cho, and M.-J. Youn, "An MRAS–based diagnosis of open–circuit fault in PWM voltage–source inverters for PM synchronous motor drive systems," *IEEE Trans. Power Electron.*, vol. 28, no. 5, pp. 2514–2526, May 2013.

[7] Z. Gao, C. Cecati, and S. X. Ding, "A survey of fault diagnosis and fault-tolerant techniques—Part I: Fault diagnosis with model-based and signal-based approaches," *IEEE Trans. Ind. Electron.*, vol. 62, no. 6, pp. 3757–3767, Jun. 2015.

[8] Z. Gao, C. Cecati, and S. Ding, "A survey of fault diagnosis and fault–tolerant techniques—Part II: Fault diagnosis with knowledge–based and hybrid/active approaches," *IEEE Trans. Ind. Electron.*, vol. 62, no. 6, pp. 3768–3774, Jun. 2015.

[9] P. Sobanski and M. Kaminski, "Application of artificial neural networks for transistor open-circuit fault diagnosis in three-phase rectifiers," *IET Power Electron.*, vol. 12, no. 9, pp. 2189–2200, Aug. 2019.

[10] T. Shi, Y. He, T. Wang, and B. Li, "Open switch fault diagnosis method for PWM voltage source rectifier based on deep learning approach," *IEEE Access*, vol. 7, pp. 66595–66608, 2019.

[11] Q.-T. An, L. Sun, and L.-Z. Sun, "Current residual vector–based open–switch fault diagnosis of inverters in PMSM drive systems," *IEEE Trans. Power Electron.*, vol. 30, no. 5, pp. 2814–2827, May 2015.

[12] B. Gou, X. Ge, S. Wang, X. Feng, J. B. Kuo, and T. G. Habetler, "An open–switch fault diagnosis method for single–phase PWM rectifier using a model–based approach in high–speed railway electrical traction drive system," *IEEE Trans. Power Electron.*, vol. 31, no. 5, pp. 3816–3826, May 2016.

[13] J. Poon, P. Jain, I. C. Konstantakopoulos, C. Spanos, S. K. Panda, and S. R. Sanders, "Model-based fault detection and identification for switching power converters," *IEEE Trans. Power Electron.*, vol. 32, no. 2, pp. 1419–1430, Feb. 2017.

[14] M. Shahbazi, P. Poure, S. Saadate, and M. R. Zolghadri, "FPGA–based reconfigurable control for fault–tolerant back-to-back converter without redundancy," *IEEE Trans. Ind. Electron.*, vol. 60, no. 8, pp. 3360–3371, Aug. 2013.

[15] R. De Araujo Ribeiro, C. Jacobina, E. Da Silva, and A. Lima, "Fault detection of open-switch damage in voltage-fed PWM motor drive systems," *IEEE Trans. Power Electron.*, vol. 18, no. 2, pp. 587–593, Mar. 2003.

[16] S. Karimi, A. Gaillard, P. Poure, and S. Saadate, "FPGA–based real–time power converter failure diagnosis for wind energy conversion systems," *IEEE Trans. Ind. Electron.*, vol. 55, no. 12, pp. 4299–4308, Dec. 2008.

[17] Q.-T. An, L.-Z. Sun, K. Zhao, and L. Sun, "Switching function model–based fast–diagnostic method of open–switch faults in inverters without sensors," *IEEE Trans. Power Electron.*, vol. 26, no. 1, pp. 119–126, Jan. 2011.

[18] Q. An, L. Sun, and L. Sun, "Hardware-circuit-based diagnosis method for open-switch faults in inverters," *Electron. Lett.*, vol. 49, no. 17, pp. 1089–1091, Aug. 2013.

[19] J. O. Estima and A. J. Marques Cardoso, "A new approach for real–time multiple open–circuit fault diagnosis in voltage–source inverters," *IEEE Trans. Ind. Appl.*, vol. 47, no. 6, pp. 2487–2494, Nov. 2011.

[20] W. S. Im, J. M. Kim, D. C. Lee, and K. B. Lee, "Diagnosis and fault-tolerant control of three-phase AC-DC PWM converter systems," *IEEE Trans. Ind. Appl.*, vol. 49, no. 4, pp. 1539–1547, Jul./Aug. 2013.

[21] F. Wu, J. Zhao, Y. Liu, D. Zhou, and H. Luo, "Primary source inductive energy analysis based real–time multiple open–circuit fault diagnosis in two–level three–phase PWM boost rectifier," *IEEE Trans. Power Electron.*, vol. 33, no. 4, pp. 3411–3423, Apr. 2018.

[22] Z. Jian-Jian, C. Yong, C. Zhang-Yong, and Z. Anjian, "Open–switch fault diagnosis method in voltage–source inverters based on phase currents," *IEEE Access*, vol. 7, pp. 63619–63625, May 2019.

[23] A. M. S. Mendes and A. J. Marques Cardoso, "Voltage source inverter fault diagnosis in variable speed AC drives, by Park's vector approach," in *Proc. Power Electron. Variable Speed Drives*, Sep. 1998, pp. 538–543.
[24] A. Mendes and A. Marques Cardoso, "Voltage source inverter fault diagnosis in variable speed AC drives, by the average current Park's vector approach," in *Proc. IEEE Int. Electr. Mach. Drives Conf. (IEMDC)*, Jan. 2003, pp. 704–706.
[25] K. Rothenhagen and F. Fuchs, "Performance of diagnosis methods for IGBT open circuit faults in three phase voltage source inverters for AC variable speed drives," in *Proc. Eur. Conf. Power Electron. Appl.*, 2005, pp. 1–10.
[26] N. M. A. Freire, J. O. Estima, and A. J. Marques Cardoso, "Open–circuit fault diagnosis in PMSG drives for wind turbine applications," *IEEE Trans. Ind. Electron.*, vol. 60, no. 9, pp. 3957–3967, Sep. 2013.
[27] F. Wu and J. Zhao, "Current similarity analysis–based open–circuit fault diagnosis for two–level three–phase PWM rectifier," *IEEE Trans. Power Electron.*, vol. 32, no. 5, pp. 3935–3945, May 2017.
[28] T. Shi, Y. He, F. Deng, J. Tong, T. Wang, and L. Shi, "Online diagnostic method of open-switch faults in PWM voltage source rectifier based on instantaneous AC current distortion," *IET Electr. Power Appl.*, vol. 12, no. 3, pp. 447–454, Mar. 2018.
[29] T. Shi, Y. He, T. Wang, J. Tong, B. Li, and F. Deng, "An improved open–switch fault diagnosis technique of a PWM voltage source rectifier based on current distortion," *IEEE Trans. Power Electron.*, vol. 34, no. 12, pp. 12212–12225, Dec. 2019.
[30] S.-H. Song, J.-W. Choi, and S.-K. Sul, "Current measurements in digitally controlled AC drives," *IEEE Ind. Appl. Mag.*, vol. 6, no. 4, pp. 51–62, Jul./Aug. 2000.

CHUNSONG SUI was born in Shandong, China, in 1996. He received the B.S. degree from the School of Electrical Engineering and Automation, Wuhan University, Wuhan, China, in 2018, where he is currently pursuing the M.S. degree in electrical engineering.

His current research interest includes fault diagnosis and fault-tolerant control for voltage source converters.

YIGANG HE (Member, IEEE) received the M.Sc. degree in electrical engineering from Hunan University, Changsha, China, in 1992, and the Ph.D. degree in electrical engineering from Xi'an Jiaotong University, Xi'an, China, in 1996.

In 1990, he joined the College of Electrical and Information Engineering, Hunan University, where he was promoted as an Associate Professor and a Professor, in 1996 and 1999, respectively. From 2006 to 2011, he worked as the Director of the Institute of Testing Technology for Circuits and Systems, Hunan University. He was a Senior Visiting Scholar with the University of Hertfordshire, Hatfield, U.K., in 2002. From 2011 to 2017, he worked as the Head of the School of Electrical Engineering and Automation, Hefei University of Technology. On December 2017, he joined Wuhan University, China, where he currently works as the Vice-Head of the School of Electrical Engineering and Automation. Meanwhile, he was the Vice President of the China's Energy Institute of Science and Technology and the Anhui Scientists Entrepreneurs Association, and the Director of the State-Local Joint Engineering Laboratory for Renewable Energy Grid Technology. His teaching and research interests are in the areas of power electronic circuit theory and its applications, testing and fault diagnosis of analog and mixed-signal circuits, electrical signal detection, smart grid, satellite communication monitoring, and intelligent signal processing. On the above research areas, he has presided over a number of state-level projects research such as the National Natural Science Foundation of China, the State Key Program of National Natural Science Foundation of China, the National Key Research and Development Plan Important Scientific Instruments and Equipment Development the National High Technology Research and Development Program of China, and the Major State Basic Research Development Program of China. He has published some 300 journal and conference papers which were included more than 1000 times in the Science Citation Index of American Institute for Scientific Information in the aforementioned areas and several chapters in edited books.

Dr. He was a recipient of a number of national and international awards, prizes, and honors. For example, he was the winner of the National Outstanding Youth Science Fund and China National Excellent Science and Technology Worker. He has been the General Chair, a Session Chair, and a Committee Member of a lot of international academic conferences, respectively.

MINGYUN CHEN was born in Zhejiang, China, in 1996. She received the B.S. degree from the School of Control Engineering, Northeastern University at Qinhuangdao, Qinhuangdao, China, in 2019. She is currently pursuing the M.S. degree in electrical engineering with the School of Electrical Engineering and Automation, Wuhan University.

Her research interests include fault diagnosis and fault-tolerant control for converters, and failure prediction.